Initiation of secondary ice production in clouds

Sylvia C. Sullivan[1], Corinna Hoose[2], Alexei Kiselev[2], Thomas Leisner[2], and Athanasios Nenes[1,3,4,5]

[1]School of Chemical and Biomolecular Engineering, Georgia Institute of Technology, Atlanta, GA 30332, USA
[2]Institute of Meteorology and Climate Research, Karlsruhe Institute of Technology, Karlsruhe, Germany
[3]School of Earth and Atmospheric Sciences, Georgia Institute of Technology, Atlanta, GA 30332, USA
[4]ICE-HT, Foundation for Research and Technology, Hellas, 26504 Patras, Greece
[5]IERSD, National Observatory of Athens, P. Penteli, 15236, Athens, Greece

Correspondence to: A. Nenes (athanasios.nenes@gatech.edu)

Abstract. Disparities between the measured concentrations of ice-nucleating particles (INP) and in-cloud ice crystal number concentrations (ICNC) have led to the hypothesis that mechanisms other than primary nucleation form ice in the atmosphere. Here, we model three of these secondary production mechanisms – rime splintering, frozen droplet shattering, and collisional breakup – with a six-hydrometeor-class parcel model. We perform three sets of simulations to understand temporal evolution of ice hydrometeor number (N_{ice}), thermodynamic limitations, and the impact of parametric uncertainty when secondary production is active. Output is assessed in terms of the number of primarily nucleated ice crystals that must exist before secondary production initiates ($N_{\text{INP}}^{(lim)}$), as well as the ICNC enhancement from secondary production and the timing of a 100-fold enhancement. N_{ice} evolution can be understood in terms of collision-based non-linearity and the 'phasedness' of the process, i.e., whether it involves ice hydrometeors, liquid ones, or both. Collisional breakup is the only process for which a meaningful $N_{\text{INP}}^{(lim)}$ exists (0.002 L^{-1} up to 0.07 L^{-1}). For droplet shattering and rime splintering, a warm enough cloud base temperature and modest updraft are the more important criteria for initiation. The low values of $N_{\text{INP}}^{(lim)}$ here suggest that, under appropriate thermodynamic conditions for secondary ice production, perturbations in CCN concentrations are more influential on mixed-phase partitioning than those in INP concentrations.

1 Background

Number concentrations of ice-nucleating particles (N_{INP}) in the atmosphere span orders of magnitude from a few per cubic meter up to 100s per liter (e.g., DeMott et al., 2010). At temperatures greater than about -15°C, these concentrations remain low: only one particle in every 10^3 or 10^4 will nucleate an ice crystal Rogers et al. (1998); Chubb et al. (2013); DeMott et al. (2015). However, even when INP concentrations are low at warm subzero temperatures, in-cloud ice crystal number concentrations (ICNC) can be orders of magnitude higher (e.g., Hallett and Mossop, 1974; Heymsfield and Willis, 2014; Lasher-Trapp et al., 2016; Taylor et al., 2016; Ladino et al., 2017), particularly in tropical maritime clouds Koenig (1963, 1965); Hobbs and Rangno (1990).

This discrepancy may be explained in some cases by shattering upon cloud probe tips (Field et al., 2003; Heymsfield, 2007; McFarquhar et al., 2007), but even as instrumentation and algorithms have been developed to minimize these artifacts (Korolev

et al., 2013; Korolev and Field, 2015), the disparity has remained, supporting several hypothesized secondary ice production processes. Hallett and Mossop (1974) proposed rime splintering in which ice hydrometeors collide with and freeze supercooled droplets to form rime, which then splinters off as the hydrometeor continues to fall. Droplets in cases of rime splintering tend to be both less than 13 μm and greater than 25 μm in diameter, and temperatures fall between -3 and -8°C (Mossop, 1978; Heymsfield and Mossop, 1984; Mossop, 1985); however, ICNC enhancement, i.e., the increase in ICNC beyond that generated by primary nucleation, exists even outside of these conditions.

Another hypothesized mechanism is the shattering of droplets with a diameter of 50 to 100s of μm upon freezing (Mason and Maybank, 1960; Scott and Hobbs, 1977; Phillips et al., 2001; Fridlind et al., 2007; Leisner et al., 2014; Lawson et al., 2015). At sufficiently cold temperatures, latent heat release leads to the formation of a liquid core-ice shell structure that eventually shatters upon internal pressure build-up. A third mechanism, independent of the liquid phase, is breakup upon mechanical collision of ice hydrometeors. Vardiman (1978) calculated the fragment number generated during collisional breakup from a change in momentum, and Takahashi et al. (1995) later conducted experiments with a rotating ice sphere in a cloud chamber to estimate the number of ice crystals ejected versus temperature. Yano and Phillips (2011), and more recently Yano et al. (2015), have identified 'explosive regimes' defined by non-dimensional parameters, where collisional breakup may enhance ICNC by as much as 10^4.

Laboratory and in-situ data of these processes are difficult to obtain, and their fragment generation functions and temperature dependence remain uncertain (Field et al., 2017). Given these uncertainties, implementation of secondary ice production parameterizations in large-scale models would be premature. Instead, small-scale , more controllable modeling provides a good tool to estimate variability of secondarily-produced ICNC with these parameters, as well as the minimum number of INP needed to initiate secondary production. This latter variable is called $N_{\mathrm{INP}}^{(lim)}$ hereafter.

Some previous studies have estimated $N_{\mathrm{INP}}^{(lim)}$ on the basis of in-situ data. For example in a study of ice initiation in cumulus, Beard (1992) found that a nucleated ICNC of 0.001 L^{-1} could trigger raindrop freezing around -5°C . More recently, Crawford et al. (2012), with Aerosol Properties, PRocesses And InFluenceS (APPRAISE) campaign data, and Huang et al. (2017), with Ice and Precipitation Initiation in Cumulus (ICEPIC) campaign data, identified a primarily nucleated ICNC of 0.01 L^{-1} as sufficient to initiate rime splintering. Connolly et al. (2006a) found that the rime splintering tendency increased with increasing primarily-nucleated ICNC, but this result was based upon adjusting the primary nucleation rate rather than the absolute N_{INP}. Clark et al. (2005) also adjusted the primary nucleation rate relative to the rime splintering one, but gave no approximate $N_{\mathrm{INP}}^{(lim)}$ values or thermodynamic constraints. These studies have also considered only rime splintering, despite evidence that multiple processes occur simultaneously (Rangno and Hobbs, 2001). We provide more comprehensive estimates of $N_{\mathrm{INP}}^{(lim)}$ here for three secondary production processes over a range of fragment numbers and thermodynamic conditions.

2 Parcel model

To estimate ICNC enhancements and $N_{\mathrm{INP}}^{(lim)}$, we run a parcel model with six hydrometeor classes for small ice crystals and droplets, small and large graupel, and medium and large droplets (Sullivan et al., 2017). The number in these classes

is denoted N_i, N_d, N_g, N_G, N_r, and N_R respectively. The hydrometeors in each class are assumed monodisperse, but their sizes are tracked over time as a function of temperature and superaturation. N_{ice} is used to denote the summation of the number in the three ice hydrometeor classes. The bin microphysics consists of primary nucleation and secondary production by collisional breakup, rime splintering, and frozen droplet shattering. An ice generation function is defined to include both primary nucleation and secondary production sources of ice crystals, with units of $\text{m}^{-3}\ \text{s}^{-1}$:

$$G_{ice} = \left.\frac{dN_i}{dt}\right|_{NUC} + \left.\frac{dN_i}{dt}\right|_{BR} + \left.\frac{dN_i}{dt}\right|_{RS} + \left.\frac{dN_i}{dt}\right|_{DS} \tag{1}$$

$$= c_0 + \eta_{BR} K_{BR} \aleph_{BR} N_g N_G + \eta_{RS} \aleph_{RS} \left[K_{RS,g} N_g + K_{RS,G} N_G \right] N_R + \eta_{DS} \aleph_{DS} N_R \tag{2}$$

c_0 is the primary nucleation rate derived from the temperature dependence of the immersion INP concentration given in DeMott et al. (2010); η_X is the weighting for process X, either 100% when the process is active or 0% when it is inactive; K_X is a gravitational collection kernel for process X; and $\aleph_X$ is the fragment number generated by process X. More specifically, the nucleation rate is calculated as the product of updraft velocity, an assumed lapse rate of 6 K km^{-1}, and the temperature derivative of the INP concentration: $u_z \Gamma d/dT \left[a_1 \exp(a_2 (T - a_3)) \right]$. This formulation requires no explicit treatment of aerosol. The specific forms of $\aleph_X$ are given in Table S1; in particular, $\aleph_{DS}$ contains a product of droplet freezing and shattering probabilities, p_{fr} and p_{sh}.

BR stands for collisional breakup, DS for droplet shattering, and RS for rime splintering. The droplet shattering tendency is later modified to represent a collisional process with a product of large droplet and ice crystal numbers and then denoted $DScoll$. η_{RS} is set to 1% outside the optimal rime splintering temperature zone of -3 to -8°C. For the liquid phase, a droplet generation function consists simply of droplet activation, calculated from a Twomey power-law formulation: droplet number is calculated solely from supersaturation rather than a CCN number. The number balance in each class is then the generation function at the current time as a source and the generation function at a time delay as the sink, along with aggregation and coalescence losses. For example, the number in the ice crystal class is given by

$$\frac{dN_i}{dt} = G_{ice}(t) - G_{ice}(t - \tau_i) - \eta_{agg} K_{agg} N_i N_g. \tag{3}$$

The time delays, τ_X, quantify how long depositional, riming, or condensational growth to the next hydrometeor class will take and are solved for approximately from growth equations. The six hydrometeor number tendencies are solved with an explicit Runge-Kutta (2,3) pair for delay differential equations (Bogacki and Shampine, 1989) and coupled to moist thermodynamic equations for pressure, temperature, supersaturation, mixing ratios, and hydrometeor sizes. This second set of equations is solved with a Rosenbrock formula of order 2 (Rosenbrock, 1963). The coalescence efficiency is assumed to be unity between small and medium droplets and negligible between two droplets of the same size (Klett and Davis, 1973). Newly produced ice crystals are assumed to be spherical with bulk ice density, while graupel is assumed to be spheroidal with a deposition density and non-unit capacitance as in Chen and Lamb (1994). The model microphysics is shown schematically in Figure S1, and parameter values and sources are given in Table S1. Model assumptions, thermodynamic tendencies and correlations, and collection kernels are more thoroughly discussed in Sullivan et al. (2017).

3 Simulations

The three rows of Table 1 show three sets of simulations with the parcel model. First we investigate the evolution of the total ice hydrometeor number, N_{ice}, i.e. the summation of N_i, N_g, and N_G, in default simulations with fixed fragment numbers and thermodynamic conditions. Simulation acronyms include BR for collisional breakup, DS for droplet shattering, RS for rime splintering, or ALL if all processes are active (see also Table 1 caption). These runs address how the value of $N_{\text{INP}}^{(lim)}$ and enhancement magnitude or timing vary when different processes are active. We quantify enhancement from secondary production as the ratio of the total ICNC to the number generated by primary nucleation when the simulation ends, i.e., when the parcel becomes water subsaturated or reaches a temperature of 237 K above which no homogeneous nucleation occurs: $N_{\text{ice}}^{(max)}/N_{\text{INP}}(t_{end})$. An enhancement of 10 can be understood as *at least* a 10-fold increase in ICNC due to secondary production, as an aggregation sink is also active in the simulations. In the absence of secondary production, ICNC enhancement does not exceed one.

The second set of simulations considers the effect of updraft velocity and initial temperature in the parcel; this set is denoted 'th' for thermodynamics. The updraft is varied from 0.1 up to 4 m s^{-1} to simulate both stratiform and convective conditions, while the initial parcel temperature is adjusted from just below the melting temperature (272 K) down below the peak of the droplet shattering probability distribution (256 K). These conditions also ensure numerical stability, given the stiffness of the coupled equations. The final set, denoted 'pp', performs parameter perturbations. In particular, we vary the leading coefficient of the fragment number generated per collision and per kilogram of rime, F_{BR} and F_{RS} respectively; the minimum temperature for which collisional breakup occurs, T_{min}; the functional form of the fragment number generated per shattering droplet, $F_{DS}(\beta,\gamma)$; and the maximum of the temperature-dependent droplet shattering probability distribution, $p_{sh}^{(max)}$. The effect of these parameters on the generated fragment numbers is shown in Figure S2, and the alternate sigmoid functional forms for $\aleph_{DS}$ are shown in Figure S3.

3.1 Hydrometeor number evolution

The temporal evolution of N_{ice} in the default simulations is shown in Figure 1. Each simulation is done for a range of total INP number within the parcel, $N_{\text{INP}}^{(tot)}$. These varying values of $N_{\text{INP}}^{(tot)}$ are shown in different colors in panel **(d)** of Figure 1. The structure in the number evolution can be understood by considering whether the process is collisional and its 'phasedness', i.e., whether it involves hydrometeors in the liquid or ice phase or both. The ice mass mixing ratio and ice crystal radius evolution are also shown in Figures S5 and S6, but analysis focuses on N_{ice} below.

When the process involves a product of hydrometeor numbers, as for breakup and rime splintering, the N_{ice} evolution is non-linear. Independent of $N_{\text{INP}}^{(tot)}$, N_{ice} grows steadily throughout the simulation for these collisional secondary production processes. Even as graupel or large droplets are consumed, those hydrometeors still in the parcel continue to grow by deposition or condensation respectively. This ongoing hydrometeor growth increases the secondary production tendencies via their collection kernels, and this link itself is non-linear because both hydrometeor terminal velocity and collisional cross section increase with growth. This idea is shown qualitatively in the red and blue traces of Figure 8a.

Table 1. All simulations with parameters adjusted from the default values in Table S1. A control run with no secondary production, i.e., $\eta_{DS} = \eta_{BR} = \eta_{RS}$ = 0%, is denoted INP in Figure 1. Thermodynamic simulations run with combinations (BRDSth, BRRSth, and DSRSth) or all (ALLth) of the processes are shown solely in the Supplement and detailed in Table S2.

Run BR	***Run DS***	***Run RS***
	(Run DScoll)	
Collisional breakup	Droplet shattering only	Rime splintering
only	(Collisional droplet shattering only)	only
$\eta_{DS} = \eta_{RS} = 0\%$	$\eta_{BR} = \eta_{RS} = 0\%$	$\eta_{BR} = \eta_{DS} = 0\%$
Run BRth	***Run DSth***	***Run RSth***
Thermodynamic variations	Thermodynamic variations	Thermodynamic variations
for collisional breakup	for droplet shattering	for rime splintering
u_z = { 0.1, 0.5, 1, 1.5, 2, 2.5, 3, 3.5, 4 m s^{-1}}	T_0 = { 256, 258, 260, 262, 264, 268, 270, 272 K}	
Run BRpp	***Run DSpp***	***Run RSpp***
Parameter perturbations	Parameter perturbations	Parameter perturbations
for collisional breakup	for droplet shattering	for rime splintering
F_{BR} = {0, 90, 140, 200, 280}	F_{DS} = {25, 75}x $10^{-12}(2\,r_D)^{-4 \text{ or } -3}$	F_{RS} = {9, 15, 30, 45, 80}
	(β, γ) = { (-0.016, 500), (-0.015, 400)}	x 10^7 (kg rime)$^{-1}$
T_{min} = {246, 249, 252, ...	$p_{sh}^{(max)}$ = {1, 5, 10, 20, 30%}	
255, 258 K}		

When the process involves a single hydrometeor number, as for this case of droplet shattering, the N_{ice} evolution is linear and does not grow steadily. Instead it exhibits threshold behavior when the temperature becomes cold enough for a non-negligible freezing probability according to Bigg (1953). A decrease in N_{ice} occurs right before the sudden increase for the DS simulation because large graupel begin to fall out of the parcel around 45 minutes. In more recent measurements with evidence of droplet shattering, the cloud base temperature has been warmer, and the updraft stronger,than the default conditions in Table S1 (e.g., Lawson et al., 2015; Taylor et al., 2016) (see Table 2). We show the N_{ice} evolution from a 'warm-base-convective' sensitivity run in Figure S7. Here the same threshold behavior occurs once the parcel reaches cold enough temperatures for droplet freezing, but there is no N_{ice} decrease beforehand because ice nucleation begins later, and no graupel has begun to fall out. Later we also model collisional droplet shattering ($DScoll$), a steady increase appears again, as explained below in Section 3.1.1. These trends are shown qualitatively in the green traces of Figure 8a.

Because breakup and rime splintering involve the ice phase, increasing $N_{\text{INP}}^{(tot)}$ boosts their rates of generation and yields large enhancements sooner. For collisional breakup, a parcel with 0.0129 L^{-1} INP reaches 10 $\text{L}^{-1} N_{\text{ice}}$ in 23 minutes, while that with 0.167 L^{-1} INP reaches the same value in 17 minutes. For rime splintering, the same increase in INP shifts the time to reach 10 L^{-1} N_{ice} from 30 minutes back to 25. While these differences in enhancement timing sound small, they can help infer which secondary production processes are active from in-situ N_{INP} and ICNC data. For example, ICNC on the order of hundreds per liter can form within 10 to 15 minutes (Hobbs and Rangno, 1990; Rangno and Hobbs, 1991, 1994). This timing is too rapid to be explained by rime splintering alone (Mason, 1996), in agreement with our RS simulation. Simulations with collisional breakup and rime splintering in combination, on the other hand, *are* sufficiently rapid (Fig. S4b).

Higher $N_{\text{INP}}^{(tot)}$ only increases the ice generation rates from collisional breakup and rime splintering up to a certain point however. Beyond an $N_{\text{INP}}^{(tot)}$ of about 0.599 L^{-1}, additional INP do not increase $N_{\text{ice}}^{(max)}$. The parcel is in a supersaturation-limited regime, for which it becomes subsaturated before the effect of additional primary nucleation can be felt by secondary production.

Finally non-linearity and hydrometeor phases involved determine enhancement magnitude. The collisional breakup tendency is proportional to the product of two ice hydrometeor numbers, N_g and N_G, so the impact of varying $N_{\text{INP}}^{(tot)}$ is most pronounced for the BR simulations. Increasing $N_{\text{INP}}^{(tot)}$ by two orders of magnitude (0.001 to 0.167 L^{-1}) increases $N_{\text{ice}}^{(max)}$ by four order of magnitude (0.0023 to 37.6 L^{-1}). The rime splintering and droplet shattering tendencies are proportional to N_R which is around 10^6 times as large as N_g or N_G, so the impact of $N_{\text{INP}}^{(tot)}$ for these processes is diluted. For the purely liquid-phase droplet shattering, the two-order-of-magnitude increase in $N_{\text{INP}}^{(tot)}$ has no significant impact on $N_{\text{ice}}^{(max)}$. For rime splintering, it actually translates to a two-fold decrease in $N_{\text{ice}}^{(max)}$ (30.58 to 16.67 L^{-1}). This decrease is the result of an increasing denominator in the $N_{\text{ice}}^{(max)}/N_{\text{INP}}(t_{end})$ expression (see also the RS panels of Figures 3 and 4 below). The rime splintering tendency is strong enough that it always generates additional ice crystals, so increasing $N_{\text{INP}}^{(tot)}$ actually decreases enhancement. The total INP number does, however, affect which rimers contribute to enhancement: when $N_{\text{INP}}^{(tot)}$ exceeds 0.167 L^{-1}, only rime splintering of small graupel can occur before subsaturation of the parcel.

3.1.1 Collisional droplet shattering

As an extension of the default simulations only, we consider N_{ice} evolution and enhancement from droplet shattering as a collisional process; no parameter perturbations or varying thermodynamics are run for this collisional formulation. In this case, the droplet shattering tendency is adjusted to be proportional to both N_R and N_i, rather than just N_R in the final term of Equation 2:

$$\left.\frac{dN_i}{dt}\right|_{DS} = \eta_{DS} K_{DS} \aleph_{DS}^{(coll)} N_R N_i \tag{4}$$

The fragment number from Lawson et al. (2015) ($F_{DS} D_R^4$) and p_{sh} are retained as in the DS simulation, but p_{fr} is removed with the understanding that the ice crystal-droplet collision initiates the freezing.

In Figure 2a, the threshold behavior of the enhancement from pure liquid droplet shattering is replaced by a steady increase similar to that from rime splintering or collisional breakup. In fact, the growth in N_{ice} is now more gradual than that from RS

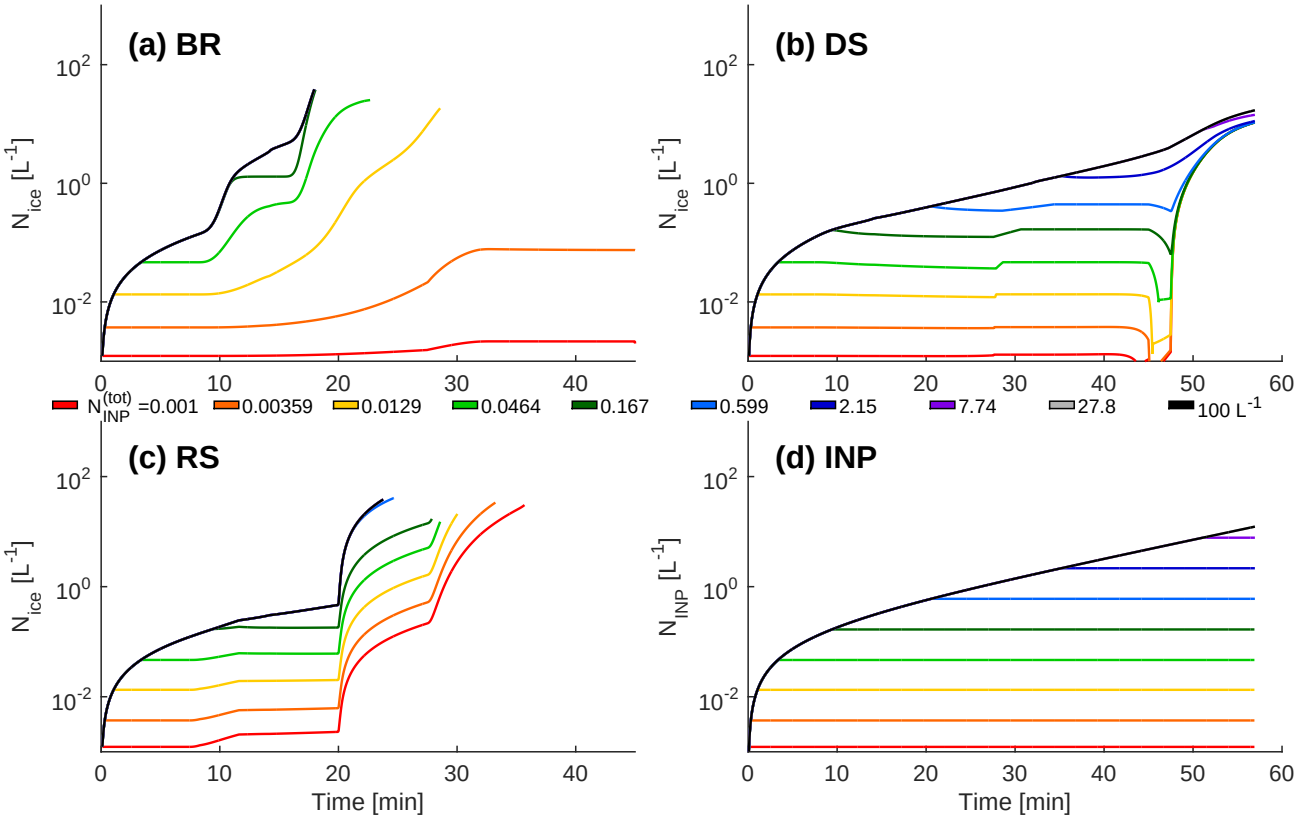

Figure 1. Evolution of the total ice hydrometeor (summation of ice crystal, small and large graupel numbers) number for default simulations with a range of $N_{\text{INP}}^{(tot)}$ from 0.001 L^{-1} up to 100 L^{-1}: **(a)** collisional breakup only, **(b)** droplet shattering only, **(c)** rime splintering only, and **(d)** a control run when only primary nucleation is active. These default simulations are run for u_z of 2 m s^{-1} and T_0 of 272 K.

or BR because N_i is also consumed by collisions now; there is effectively a linear increase in log space as $dN_i/dt \propto N_i$. This combined source and sink of N_i from droplet shattering also yields a smaller $N_{\text{ice}}^{(max)}$ of only 3.47 L^{-1} when two fragments are generated per collision and 7.87 L^{-1} when 10 are generated. The enhancement timing, on the other hand, has been much accelerated to about 14 (n = 10) or 15 (n = 2) minutes. $N_{\text{INP}}^{(tot)}$ still has no meaningful effect on either enhancement magnitude or timing.

As an uppermost bound for the enhancement from droplet shattering, we rerun the DS simulation with p_{fr} set to 1. In this case, an $N_{\text{ice}}^{(max)}$ of 17.67 L^{-1} is obtained over 27.8 minutes, not as fast as the collisional droplet shattering but about twice as fast as DS with non-unity p_{fr}. The temperature-dependent freezing probability above delays the DS enhancement, and in cases where p_{fr} is higher, droplet shattering may occur much more rapidly. Future work should also incorporate a dependence of p_{fr} on the number of submerged INP (Paukert et al., 2017), rather than just on time and temperature. Temperature and updraft dependencies are investigated in more detail next.

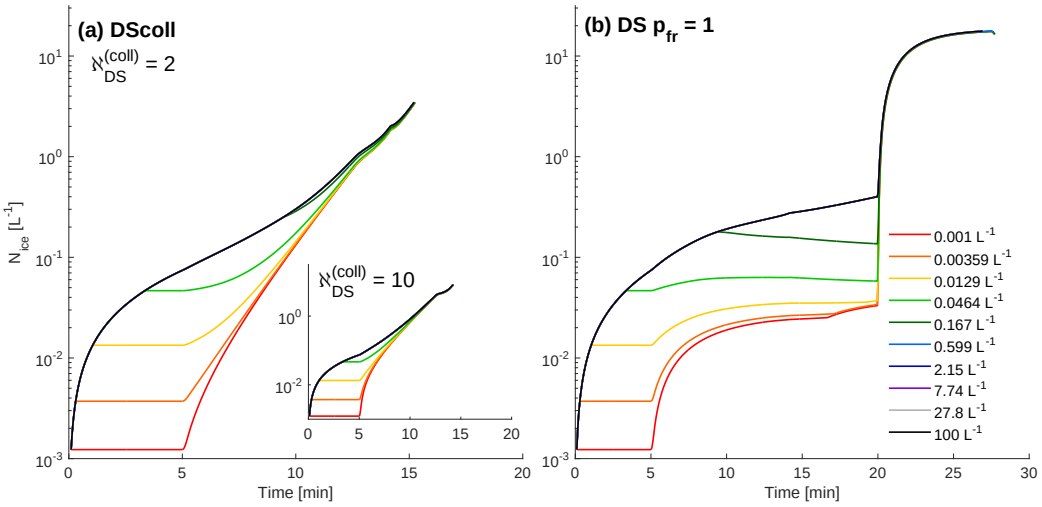

Figure 2. Evolution of N_{ice} for **(a)** collisional droplet shattering and **(b)** droplet shattering with p_{fr} of 1 over the same range of $N_{\text{INP}}^{(tot)}$ as in Figure 1. p_{sh} is set to the default value of 20%. For the main panel **(a)**, droplet shattering generates 2 fragments per collision ($\aleph_{DS}^{(coll)}$ = 2), and for the inset, 10 fragments per collision ($\aleph_{DS}^{(coll)}$ = 10). These extensions to the default simulations are run for u_z of 2 m s^{-1} and T_0 of 272 K.

3.2 Varying thermodynamics

Secondary enhancements from the simulations with varying thermodynamics are shown in Figures 3 and 4. Runs are performed for a range of updraft velocities and initial temperatures given in Table 1, but we focus on the extremes, as behavior in between is intermediate.

The top panels of Figure 3 show enhancements for stratiform conditions, i.e. u_z of 0.5 or 1 m s^{-1}, and a range of cloud base temperatures T_0. These cloud base temperatures are colder than those associated with most in-situ measurements of frozen droplet shattering (Lawson et al., 2015; Taylor et al., 2016); however, our simulations still produce droplets of sufficient diameter to shatter, $\mathcal{O}(100\ \mu\text{m})$, and a 'warm-base-convective' sensitivity run is shown in Figure S7. $N_{\text{INP}}^{(lim)}$ values for collisional breakup can be seen in panel **(a)**. As T_0 decreases from 272 to 270 to 268 K, $N_{\text{INP}}^{(lim)}$ drops from 32.8 to 21.5 to 2.1 m^{-3}. At 266 K, $N_{\text{INP}}^{(lim)}$ increases again, reaching an $\mathcal{O}(10^2)$ enhancement only for an INP concentration of 0.143 L^{-1}. Larger ICNC occur only at these warmer T_0 because the parcel remains in the mixed-phase temperature range long enough that large graupel can form (see also Figure 8b). For droplet shattering and rime splintering, there is no $N_{\text{INP}}^{(lim)}$ value greater than 1 m^{-3}: the enhancement is largest at the lowest value of $N_{\text{INP}}^{(tot)}$ in Figure 3 and decreases with higher values of $N_{\text{INP}}^{(tot)}$.

Then when u_z is increased to 4 m s^{-1} in the bottom panels, the T_0 range over which droplet shattering and rime splintering occur expands, while the enhancement magnitude shrinks. If T_0 is too cold and u_z is too strong, or conversely T_0 is too warm and u_z is too weak, the parcel does not remain in the appropriate temperature range for a long enough time to generate large hydrometeors that can shatter or collide. In particular, enhancement from collisional breakup disappears for all T_0 values at a

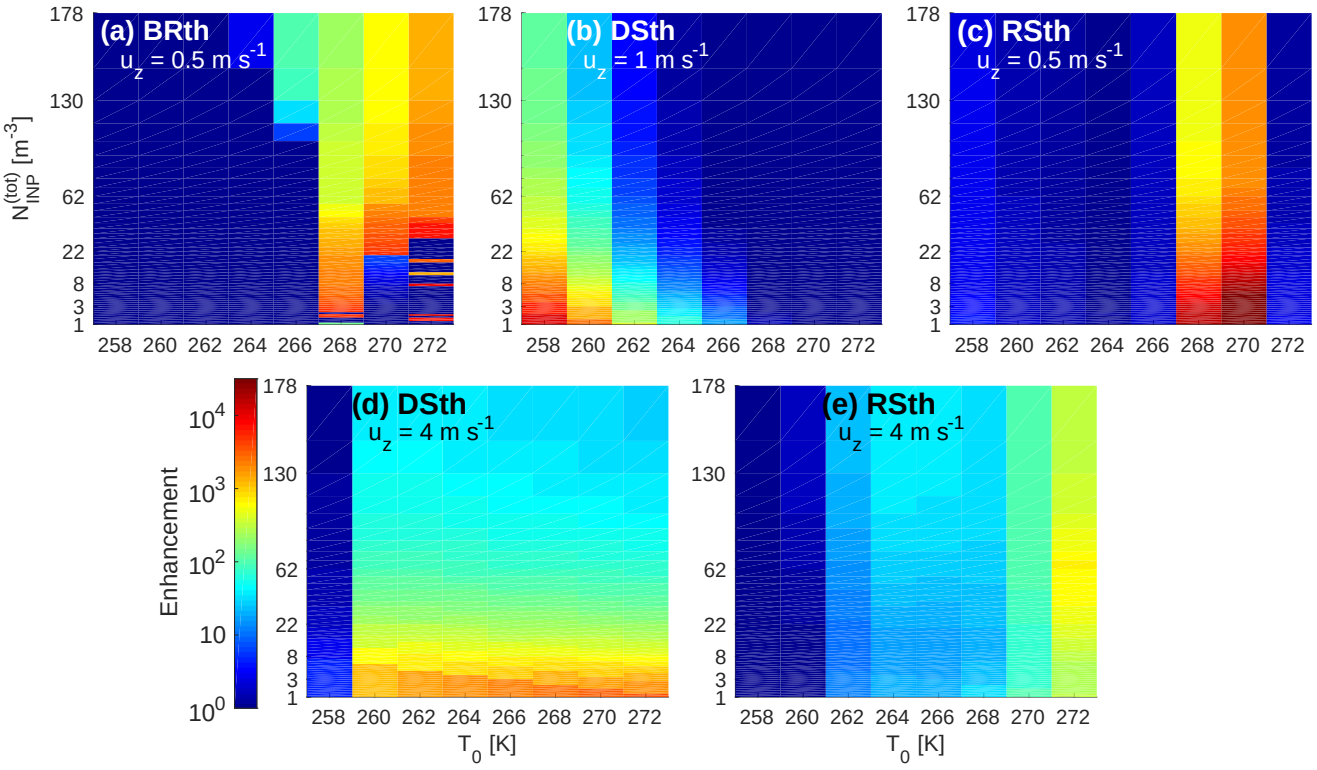

Figure 3. Ice crystal number concentration enhancement, i.e., $N_{\text{ice}}(t_{end})/N_{\text{INP}}(t_{end})$, for the thermodynamics simulations at various values of $N_{\text{INP}}^{(tot)}$, the total INP number in the parcel, and T_0, the initial temperature. Red indicates a larger enhancement per INP. Panels **(a)**, **(b)**, and **(c)** show the enhancement for collisional breakup and rime splintering at a low, stratiform-like updraft of 0.5 m s^{-1}. The lowest updraft of 0.1 m s^{-1} is not shown because only very small enhancements occur. Droplet shattering is shown at 1 m s^{-1} for the same reason. Panels **(d)** and **(e)** show the enhancement for droplet shattering and rime splintering at a higher, convective-like updraft of 3.5 m s^{-1}. No meaningful enhancements are generated by collisional breakup at this larger updraft.

larger u_z because the parcel is too short-lived for graupel to form again. As the parcel moves faster, it is more likely to pass through the 'RS temperature zone' of 267 to 269 K or obtain higher p_{sh} or p_{fr}, but it also spends less time in these optimal zones. These trends are visualized in Figures 9 and 8b.

If instead, we fix T_0 and look at a range of u_z as in Figure 4, collisional breakup remains the only process with a defined $N_{\text{INP}}^{(lim)}$. At the lowest values of $N_{\text{INP}}^{(tot)}$ for the droplet shattering and rime splintering panels, enhancements are large and decrease with increasing $N_{\text{INP}}^{(tot)}$. Only for collisional breakup does $N_{\text{INP}}^{(tot)}$ need to surpass a threshold before a large enhancement occurs. This threshold value decreases from 32.8 m^{-3} at 0.5 m s^{-1} down to 1.52 m^{-3} at 1.5 m s^{-1}. At 2.5 m s^{-1}, it increases back up to 50 m^{-3}, and at the fastest updraft velocities, no enhancement from collisional breakup occurs again because graupel does not form. In this case, not only is the parcel too short-lived for graupel formation; diffusional growth is also slowed significantly at such low temperatures.

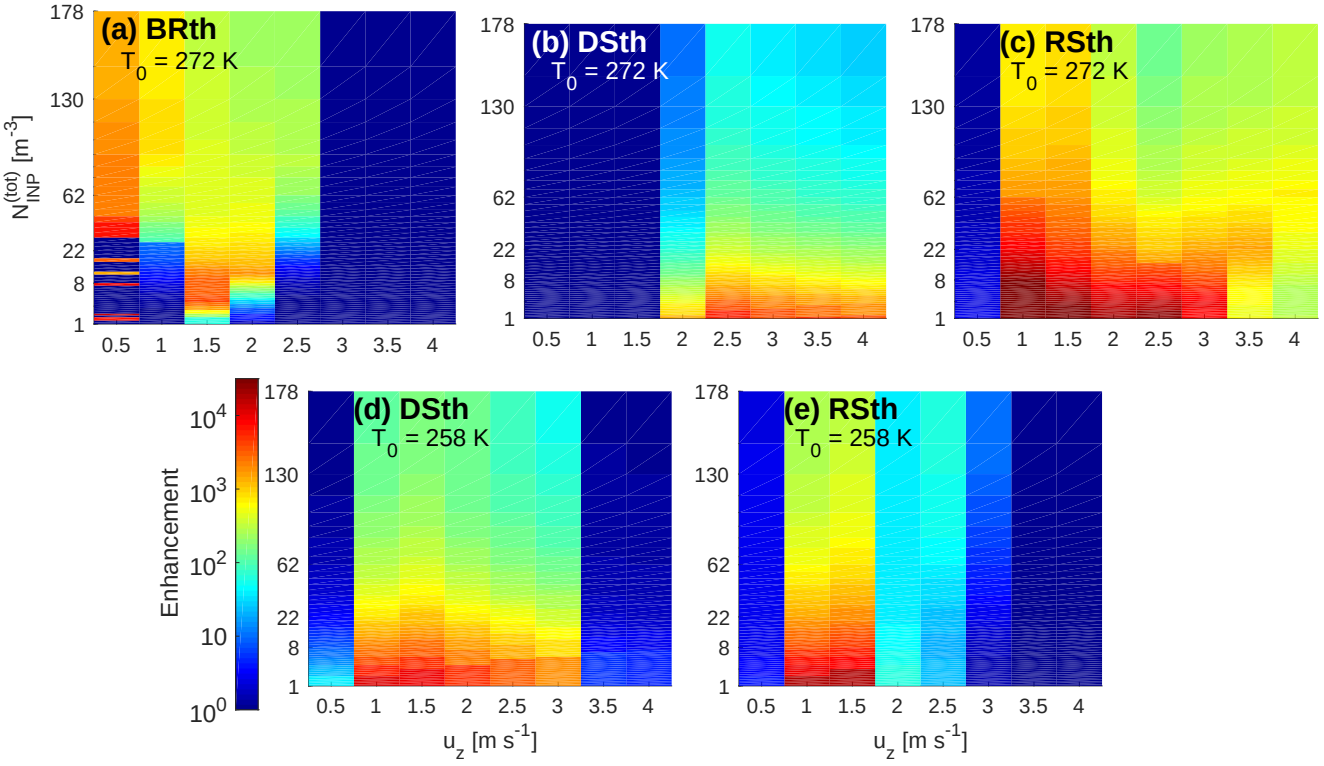

Figure 4. Ice crystal number concentration enhancement, i.e., $N_{\text{ice}}(t_{end})/N_{\text{INP}}(t_{end})$, for the thermodynamics simulations at various values of $N_{\text{INP}}^{(tot)}$, the total INP number in the parcel, and u_z, the updraft velocity. Red indicates a larger enhancement per INP. Panels **(a)**, **(b)**, and **(c)** show the enhancement for collisional breakup, droplet shattering, and rime splintering only at a warmer cloud base temperature of 272 K. Panels **(d)** and **(e)** show the enhancement for droplet shattering and rime splintering at a colder cloud base temperature of 258 K. No meaningful enhancements are generated by collisional breakup at this colder T_0.

For colder T_0, the idea of a 'sweet spot' in u_z appears again. The updraft must be strong enough that large droplets form by condensational growth but modest enough that these droplets remain in an appropriate temperature range for long enough. These trends are summarized in the first panel of Figure 9 and agree generally with Mossop (1985) in which enhancement was possible down to 0.55 m s^{-1} but highest around 1.8 to 2 m s^{-1}. Mossop used a shell-fracture hypothesis to explain this optimum: too high a velocity and the riming drop spreads across the ice surface, rather than forming a fragile protuberance, and too small a velocity and an incomplete ice shell may form around the riming drop. Although not a validation of this hypothesis, the simplified model is, interestingly, able to reproduce this u_z behavior without such detailed rime physics.

Although there is no meaningful $N_{\text{INP}}^{(lim)}$ for droplet shattering or rime splintering, N_{INP} still affects enhancement from these processes. In fact, increasing $N_{\text{INP}}^{(tot)}$ generally decreases enhancement for all $u_z - T_0$ conditions. This can be understood in terms of a sort of **INP efficiency**: the highest ICNC per INP is produced when $N_{\text{INP}}^{(tot)}$ is lowest. Mathematically, increasing $N_{\text{INP}}^{(tot)}$ increases the denominator of the enhancement ratio without a corresponding increase in the numerator. Physically,

a higher $N_{\text{INP}}^{(tot)}$ depletes supersaturation more rapidly, as many small ice crystals grow by deposition, or it may keep the parcel warmer with latent heating. Fragment numbers, $\aleph_{DS}$ and $\aleph_{RS}$, also depend on the large droplet radius or rimed mass, which are reduced at lower supersaturation. Previous work corroborates this understanding: Connolly et al. (2006a) found that increasing primary nucleation led to a decrease in the freezing of rain in cloud resolving simulations. Other studies have also emphasized the importance of liquid hydrometeor formation, rather than primary nucleation, to ice generation from rime splintering (Mossop, 1978, 1985; Hobbs and Rangno, 1985; Heymsfield and Willis, 2014).

Finally, Figures 3 and 4 show enhancement from a single process, but enhancement from multiple secondary production processes simultaneously can generally be understood as the linear combination of that from these single processes (Figures S8, S9, or S10). For example, the pattern of enhancement from ALLth in Figure S8 looks like the addition of the patterns from RSth, DSth, and BRth in Figure 3.

3.3 Parameter perturbations

Lastly we use the insight about N_{ice} evolution and approximate enhancements from the above simulations to investigate the impact of adjustable parameters. In particular, we look at the effect of generated fragment numbers and temperature dependencies on $N_{\text{INP}}^{(lim)}$ and enhancement magnitude or timing.

First the effect of nucleation rate is investigated on the $N_{\text{INP}}^{(lim)}$ value for breakup, as illustrated in Figure 5. The top panels show results from a default nucleation rate and ones reduced by factors of 10 and 100. The conditions for which no enhancement occurs are shown in black in Figure 5, and the number of these points increases dramatically as the nucleation rate decreases from left to right (8 to 32 to 84%). Then as T_{min} increases, the temperature range over which collisional breakup occurs shrinks, and $N_{\text{INP}}^{(lim)}$ increases: more ice crystals are needed initially to reach a 100-fold enhancement ultimately. As F_{BR} increases, more fragments are formed per collision, and $N_{\text{INP}}^{(lim)}$ decreases. This second effect of F_{BR} is the larger of the two. These $N_{\text{INP}}^{(lim)}$ trends for collisional breakup occur until a sufficiently low F_{BR} or sufficiently high T_{min}, beyond which enhancement does not occur for any value of $N_{\text{INP}}^{(tot)}$ (up to 300 L^{-1}).

The bottom panels show N_{ice} evolution for various values of F_{BR} and T_{min} and for $N_{\text{INP}}^{(tot)}$ of 0.0129 L^{-1} (in yellow) and 0.167 L^{-1} (in green). The effect of both parameters is much larger when $N_{\text{INP}}^{(tot)}$ is small. Increasing F_{BR} from 40 to 280 increases N_{ice} by a factor of 200 when $N_{\text{INP}}^{(tot)}$ is 0.0129 L^{-1} and by only a factor of 3 when $N_{\text{INP}}^{(tot)}$ is 0.167 L^{-1}. Similarly, decreasing T_{min} from 258 to 246 K increases N_{ice} by a factor of 230 when $N_{\text{INP}}^{(tot)}$ is 0.0129 L^{-1} and by only a factor of 1.5 when $N_{\text{INP}}^{(tot)}$ is 0.167 L^{-1}. The parameters also mostly affect the enhancement magnitude not its timing.

Then the effect of shattering probability and generated fragment number are investigated for droplet shattering. We triple the leading coefficient F_{DS} and alter the diameter dependence from quartic to cubic within the Lawson et al. (2015) formulation. We also use two sigmoids shown in Figure S3, which generate higher $\aleph_{DS}$ at small D_R and lower $\aleph_{DS}$ at large D_R relative to Lawson et al. (2015). These modifications are based on fragment numbers during droplet levitation experiments that deviate from the predictions of the Lawson et al. (2015) parameterization. As above, there is no meaningful $N_{\text{INP}}^{(lim)}$ here, so we focus on the maximum enhancement from these various cases, shown in Figure 6.

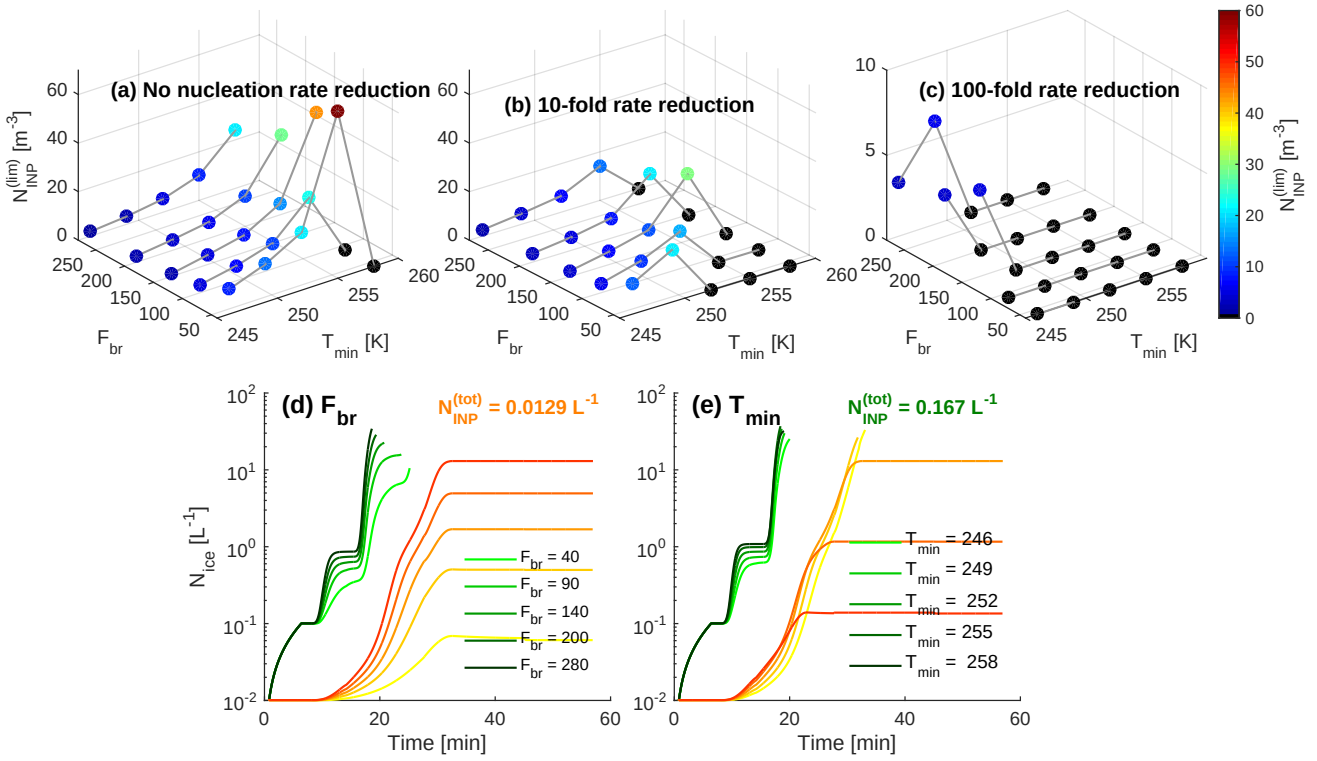

Figure 5. Results from the parameter perturbation simulations with collisional breakup. The top panels show $N_{\text{INP}}^{(lim)}$ to obtain a 100-fold enhancement in N_{ice} for various values of F_{BR} and T_{min} within the collisional breakup parameterization. Dots are also colored by $N_{\text{INP}}^{(lim)}$, where black indicates no 100-fold enhancement ever occurring. From panel **(a)** to **(b)** to **(c)**, the nucleation rate decreases by two orders of magnitude; note that the y-axis in panel **(c)** has a smaller range than the others. The bottom panels show the temporal evolution of N_{ice} for the various values of F_{BR} and T_{min} with $N_{\text{INP}}^{(tot)}$ of 0.167 L^{-1} (green traces) and 0.012 L^{-1} (yellow traces). The light-to-dark gradient in green and yellow corresponds to the same parameter values. These parameter perturbations are run for u_z of 2 m s^{-1} and T_0 of 272 K.

In panel **(a)**, by far the smallest enhancements occur for a D_R^3 dependence in $\aleph_{DS}$. Independent of $p_{sh}^{(max)}$ these simulations never produce an ICNC enhancement greater than about 50. Larger enhancements occur for the D_R^4 dependence in $\aleph_{DS}$ than for a sigmoidal dependence on D_R. Interestingly for the largest leading coefficient, F_{DS} of 7.5 x 10^{-11}, higher $p_{sh}^{(max)}$ does not monotonically increase enhancement. Another kind of 'sweet spot' exists here, and too rapid initial fragment generation may actually deplete cloud liquid faster and limit ultimate ice crystal generation (Beheng, 1987; Connolly et al., 2006b; Field et al., 2017). Elsewhere, increasing $p_{sh}^{(max)}$ does yield higher enhancement, up to about 2500 for the sigmoidal $\aleph_{DS}$ and an order of magnitude more for the default D_R^4 $\aleph_{DS}$.

Panels **(b)** and **(c)** show N_{ice} evolution for various values of $p_{sh}^{(max)}$ and the sigmoidal and default D_R^4 and $\aleph_{DS}$ forms respectively. The yellow traces show this evolution for $N_{\text{INP}}^{(tot)}$ of 0.0129 L^{-1} and the green for 0.167 L^{-1}, but these INP

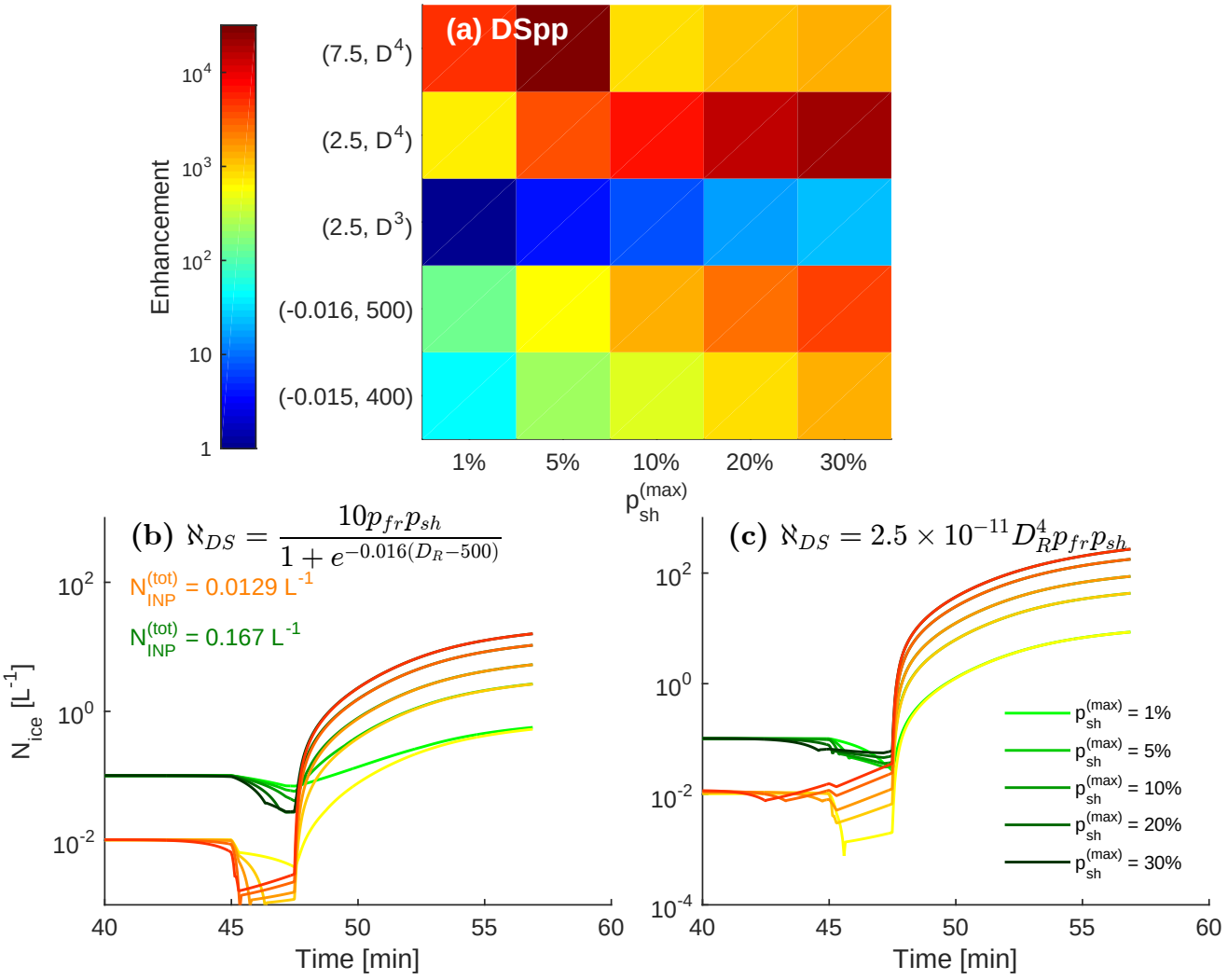

Figure 6. Results from the parameter perturbation simulations with droplet shattering. Panel **(a)** shows how the enhancement magnitude shifts with the various values of F_{DS} and p_{max}. Panels **(b)** and **(c)** show the temporal evolution of N_{ice} for the various values of F_{DS} and p_{max} with $N_{\text{INP}}^{(tot)}$ of 0.167 L^{-1} (green traces) and 0.012 L^{-1} (yellow traces). The light-to-dark gradient in green and yellow corresponds to the same parameter values. These parameter perturbations are run for u_z of 2 m s^{-1} and T_0 of 272 K.

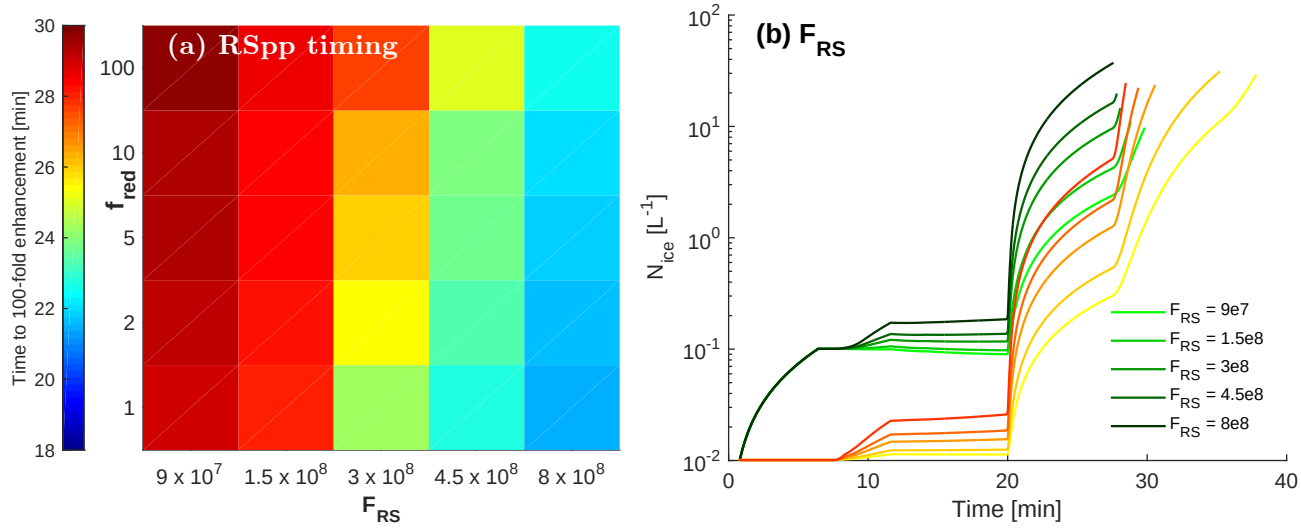

Figure 7. Results from the parameter perturbation simulations with rime splintering. Panel **(a)** shows how time of a 100-fold enhancement shifts with the fragment number per kilogram rime F_{RS} and the nucleation reduction rate f_{red}. Panel **(b)** shows the temporal evolution of N_{ice} for various values of F_{RS} with $N_{\text{INP}}^{(tot)}$ of 0.167 L^{-1} (green traces) and 0.012 L^{-1} (yellow traces). The light-to-dark gradient in green and yellow corresponds to the same parameter values. These parameter perturbations are run for u_z of 2 m s^{-1} and T_0 of 272 K.

concentrations do not make a significant difference. Again it is clear that the D_R^4 dependence generates more ice crystals. And increasing $p_{sh}^{(max)}$ by a factor of 10 from 1 to 10% translates linearly to a factor 10 increase in $N_{\text{ice}}^{(max)}$.

Finally, we investigate the impact of the fragment number from rime splintering, F_{RS}. Here we consider enhancement timing because the thermodynamic simulations show that there is no meaningful $N_{\text{INP}}^{(lim)}$ and the default ones show that the enhancement magnitude stays more or less constant. Panel **(a)** shows how the enhancement timing varies with the nucleation rate and fragment number F_{RS}. Slower nucleation rates are quantified by a reduction factor f_{red} on the y-axis. Along with lower F_{RS}, slower nucleation yields longer enhancement times, but only by about 8 minutes relative to the highest nucleation rate and F_{RS}. F_{RS} is the more influential factor in timing. Its impact on N_{ice} evolution is shown in panel **(b)**, where a given enhancement is obtained over a shorter period for a higher F_{RS}. As for collisional breakup, the effect of the parameter is much larger when $N_{\text{INP}}^{(tot)}$ is smaller in the yellow traces.

4 Discussion and observational comparison

In Table 2, the parcel model results from the previous three sections are compared to those from field and laboratory measurements for each process. Similar time frames for enhancement, $\mathcal{O}$ (30 minutes), and favorable modest updrafts and warmer cloud base temperatures are present in both the observations and simulations. The same importance of $N_{\text{INP}}^{(lim)}$ to collisional breakup has been shown in other studies (e.g. Vardiman, 1978).

An important limitation of the parcel model is the assumption of monodispersity. Large droplets shatter more effectively, and large graupel will have a larger sweep-out kernel for collisional breakup. Without the tails of a hydrometeor size distribution, these larger hydrometeors are omitted, and secondary production is underestimated. An ongoing study will implement similar formulations into a mesoscale meteorological model to understand the effect of this assumption. Ventilation effects, spatial phase separation, and continuous sedimentation are other, more advanced features of a real-world parcel that could also alter these parcel model results (Sullivan et al., 2017). For example, droplet or ice hydrometeor growth will be enhanced by the stronger vapor density gradient generated by their in-cloud motion. Again, omitting additional hydrometeor growth will underestimate secondary production. If 'pockets' of ice phase exist within mixed-phase cloud, then the values of $N_{\text{INP}}^{(lim)}$ will be more influential as the collisional breakup contribution will increase relative to rime splintering or droplet shattering. If a continuous formulation of sedimentation were substituted for the threshold one used here, the largest enhancements in Figures 3 and 4 should shift to higher updrafts. Large hydrometeors would be held aloft by these higher updrafts and feed into the secondary production tendencies. The parcel model could be extended in future studies to investigate these effects.

Table 2. Comparison of parcel model results in each section with results from in-situ and laboratory measurements not used to constrain the model formulations.

	In-situ measurements	*Laboratory studies*	*Parcel model simulations*
Temporal evolution of N_i	**BR** and **DS**: 20 min to form drizzle drops and 12-15 min to glaciation after first ice (Taylor et al., 2016); **DS**: 2-3 min to glaciation after first ice (Lawson et al., 2015); **RS**: 10^2 enhancements within 10-15 min (Hobbs and Rangno, 1990), 8 L^{-1} over 32 min (Heymsfield and Willis, 2014)	**BR**: 20 min to increase ICNC by a factor of 10 with initial ICNC of 3 L^{-1} (Vardiman, 1978) (his Fig. 7); **DS**: only 50 seconds to fragmentation after equilibration and nucleation time (Johnson and Hallett, 1968); **RS**: Linear increase starting between 10 and 20 min (Hallett and Mossop, 1974) (their Fig. 1)	**BR**: Superexponential increase based on $N_{\text{INP}}^{(tot)}$; **DS**: threshold increase based on p_{fr}; **DScoll** Exponential increase based on N_R; **RS**: Superexponential increase based on N_R
Limiting INP or thermodynamics	**BR**: T_{top} between -10° and -18°C with N_{ice} from 0.1 to 5 L^{-1} (Rangno and Hobbs, 2001); **DS** and **RS**: Taylor et al. (2016) cite the importance of the warm rain process through T_0, CDNC, u_z, and cell lifetime; **DS**: N_{INP} of 10^{-4} to 10^{-2} L^{-1} for $\overline{N_i}$ of 572 L^{-1} (Lawson et al., 2015); **RS**: $N_{\text{INP}}^{(lim)}$ of 0.01 L^{-1} (Crawford et al., 2012)	**BR**: Strong modulation of ultimate ICNC by initial ICNC (Vardiman, 1978) (his Figure 1); **DS**: $N_{\text{INP}}^{(lim)}$ of 1 m^{-3} (Beard, 1992), Favorable temperatures colder than those for RS (Korolev et al., 2004); **RS**: optimal temperatures between -3 and -8°C (Hallett and Mossop, 1974), modest updrafts are most favorable (Mossop, 1985; Heymsfield and Willis, 2014)	**BR**: $N_{\text{INP}}^{(lim)}$ from 2 up to 70 m^{-3}, possible only at warmer T_0 and slower u_z; **DS**: no meaningful $N_{\text{INP}}^{(lim)}$, favored at colder T_0 down to 258 K as u_z slows; **RS**: no meaningful $N_{\text{INP}}^{(lim)}$, favored for 268-270 K but this range widens as u_z increases
Parametric uncertainty	**BR**: In-cloud graupel collision rate of 1 m^{-3} s^{-1} (Mizuno and Matsuo, 1992), 10% of ice particles were fragmented (Rangno and Hobbs, 2001); **DS**: 10^{-9} fragments per kg liquid (Lawson et al., 2015), 10% of drops frozen by -6°C (Brownscombe and Thorndike, 1968); **RS**: 1.4 L^{-1} s^{-1} (Taylor et al., 2016), 50 crystals s^{-1} (Heymsfield and Willis, 2014)	**BR**: Fragment generation rate K_0 of 0.00081 up to 0.01 L^{-1} s^{-1} (Vardiman, 1978); **DS**: Shattering frequencies of 10 to 37% between 50 and 120 μm (Brownscombe and Thorndike, 1968; Takahashi, 1976); **RS**: 250-700 splinters per mg rime at u_z = 1.5 m s^{-1}, 200-400 at 2 m s^{-1} (Hallett and Mossop, 1974) (their Fig. 3), 90-350 (Mossop, 1985)	**BR**: 10^2-fold enhancement increasing F_{BR} from 40 to 280 at $N_{\text{INP}}^{(tot)}$ of 0.17 L^{-1}; **DS**: 10-fold enhancement increasing $p_{sh}^{(max)}$ from 1 to 30% independent of $N_{\text{INP}}^{(tot)}$; **RS**: 10 minute sooner enhancement increasing F_{RS} from 3 x 10^8 to 3 x 10^9 for all $N_{\text{INP}}^{(tot)}$

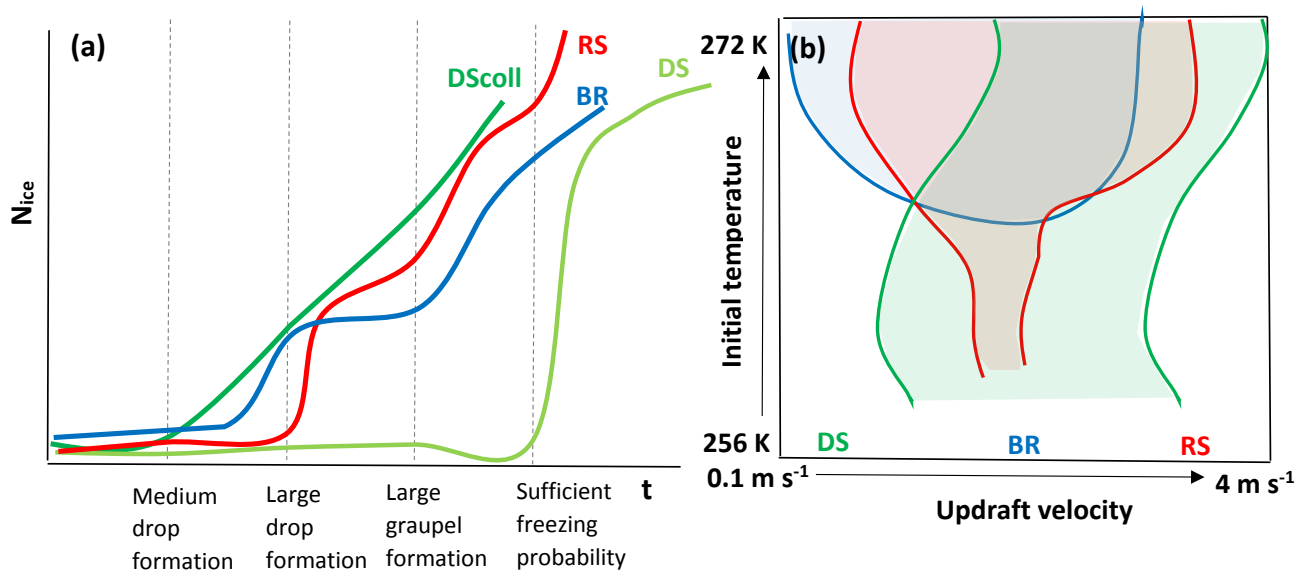

Figure 8. Qualitative summary of the findings from the default and varying thermodynamic simualtions in Section 3.1 and 3.2. Panel **(a)** summarizes N_{ice} evolution for the different processes, particularly the instances of influential hydrometeor formation and whether the process exhibits gradual or threshold increases. Panel **(b)** shows which processes are possible for conditions in the T_0-u_z space.

5 Summary and Outlook

We have performed three sets of simulations with a six hydrometeor class parcel model, considering the effect of thermodynamics and parameter perturbations on $N_{\text{INP}}^{(lim)}$, as well as ICNC enhancement and timing. Our findings can be summarized in three points:

1. *The evolution of N_{ice} from secondary production is determined by collision-based non-linearity and single versus two-phasedness.*

   N_{ice} increases gradually for the collision-based processes of breakup and rime splintering, whereas for non-collisional droplet shattering, N_{ice} increases significantly and suddenly, only when p_{fr} becomes large enough at cold enough temperatures. $N_{\text{INP}}^{(tot)}$ affects both the enhancement magnitude and timing for collisional breakup. For rime splintering, $N_{\text{INP}}^{(tot)}$ affects timing to obtain a given $N_{\text{ice}}(t_{end})$, while for droplet shattering, it has almost no impact on either magnitude or timing. These trends are summarized qualitatively in Figure 8a.

2. *$N_{INP}^{(lim)}$ can be as large as 0.07 L^{-1} for collisional breakup. Rime splintering or droplet shattering enhancement is determined by a thermodynamic 'sweet spot' rather than by $N_{INP}^{(lim)}$.*

$N_{\text{INP}}^{(lim)}$ increases for collisional breakup as the fragment number decreases or the temperature range shrinks, particularly for $N_{\text{INP}}^{(tot)}$ of 0.01 L^{-1} or less. At faster nucleation rates, the fragment number and temperature range are also more influential: enhancement occurs for 90% of the parameter space at a default nucleation rate, and just 10% of the space at a rate 100 times slower. These trends are visualized in the 'primary ice' panel of the summary schematic (Fig. 9).

For rime splintering or droplet shattering, ICNC enhancements of 10^4 are possible even for slow nucleation rates and $N_{\text{INP}}^{(tot)}$ as low as 1 m^{-3}. For these processes involving the liquid phase, an intermediate updraft for which hydrometeors grow fast enough but also spend long enough in the appropriate temperature zone is more important. The cloud base temperature must also be warm enough, i.e., greater than 260 K in our simulations. These trends are summarized visually in Figure 8b.

3. *When multiple secondary production processes are active, no single process dominates ICNC enhancement.*

   At higher nucleation rates, low u_z, and warm T_0, the contribution from collisional breakup is large. If INP are limited, u_z is somewhat higher, or T_0 is somewhat colder, droplet shattering is more important. Or if temperature falls in the optimal zone of 268 to 270 and u_z is intermediate, the rime splintering contribution will be large. A large p_{fr} for droplet shattering, however, throws off this balance. If p_{fr} is closer to unity, non-collisional droplet shattering dominates, as it depends on liquid hydrometeors only and has less stringent temperature dependence than rime splintering. This result may be inferred from the large overlap of processes in Figure 8b.

More generally, the role of ice-nucleating particles in secondary production reflects how changing aerosol emissions will affect cloud phase partitioning. The low or non-existent values of $N_{\text{INP}}^{(lim)}$ calculated in this study indicate that perturbations in CCN concentrations are more influential on mixed-phase partitioning than those in INP concentrations, with the caveat that thermodynamic conditions are appropriate for secondary production. If the mixed-phase cloud is polluted by more CCN, the higher droplet number will mean that fewer droplets reach a sufficient size to shatter or rime efficiently (This last factor has been called the riming indirect effect (Borys et al., 2003; Lance et al., 2011; Lohmann, 2017). And in these cases, the supercooled liquid fraction remains higher, and the cloud reflects more shortwave radiation. More pollution by CCN could also yield a thermodynamic indirect effect in which latent heat is released at high altitudes and strengthens the upward movement of the cloud; Koren et al. (2005) have called this cloud invigoration. Our simulations have shown that beyond a certain updraft, secondary production is no longer favored. In this way, the liquid portion of a mixed-phase cloud could also remain higher.

The impact of INP concentrations could be larger for deep convective clouds in which anvil spreading is caused by generation of many small crystals at cloud top (Fan et al., 2013). If the cloud is polluted by more INP, more vigorous secondary production by collisional breakup may occur under conditions of fast enough nucleation rate but modest enough updraft and warmer subzero cloud base temperatures. These limited conditions can be found in deep convective clouds, along with other regions favorable for secondary production like the "mixing regions" at the edges of rising turrets or tops of eroding ones (Beard,

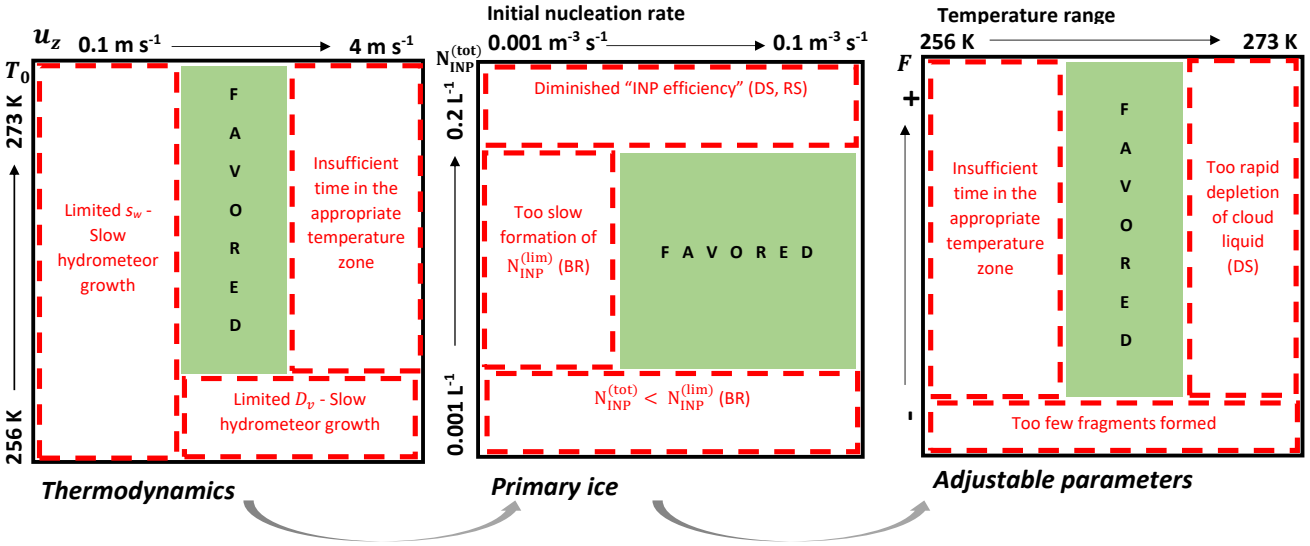

Figure 9. Summary of thermodynamic, primary ice, and adjustable parameter trends affecting ICNC enhancement from secondary production. F denotes the leading coefficient of a fragment number function for process X, $\aleph_X$. Regions in red indicate that secondary production may be limited, and those in green indicate that conditions are favorable. If the limitation is applicable only to one process, this is indicated in parentheses. The INP efficiency mentioned in the primary ice panel refers to the idea that lower secondary enhancements per INP are produced as the INP concentration increases.

1992). In contrast to the riming or thermodynamic indirect effects mentioned above, an ICNC increase at the deep convective cloud top, a kind of 'anvil enhancement effect', would radiatively warm the surface.

A systematic quantification of $N_{\mathrm{INP}}^{(lim)}$ is also relevant for the growing field of bioaerosol. Primary biological aerosol particles (PBAP) exist in the atmosphere at much lower number concentrations than dust or black carbon. But they also nucleate at warmer subzero temperatures (Hoose and Möhler, 2012; Fröhlich-Nowoisky et al., 2016), and small biological residues can intermix with dust particles to boost ice nucleation activity (Conen et al., 2011; O'Sullivan et al., 2015; Steinke et al., 2016). Even when their contribution to primarily nucleated ICNC is small, they may remain influential via initiation of secondary ice production. For example, the ice active fraction of 10^{-4} for *Pseudomonas syringae* measured by Möhler et al. (2008) around -8°C could provide the 0.01 L^{-1} seed concentration from Crawford et al. (2012) for concentrations of 10^5 m^{-3}, although this is an upper bound for bioaerosol number. From our calculations, it could also provide the $N_{\mathrm{INP}}^{(lim)}$ necessary for collisional breakup to occur. Bioaerosol could also be sufficient to initiate rime splintering, given that this process occurs even for N_{INP} below 1 m^{-3} in our simulations. A climatically important linkage has also been hypothesized between PBAP, in-cloud ICNC, and cold phase-initiated rain and is often termed the 'bioprecipitation feedback' (Huffman et al., 2013; Morris et al., 2014). The possibility of secondary production with a low $N_{\mathrm{INP}}^{(lim)}$ means that even a few bioaerosol could trigger generation of many small ice hydrometeors from larger droplets or graupel and suppress precipitation.

As a summary of our findings, we present an organizational framework for future studies of secondary production in Figure 9. Favorable conditions for large ICNC enhancements are shown in green, e.g., warmer subzero cloud base temperatures and intermediate updraft in the thermodynamic panel or higher nucleation rate for collisional breakup in the primary ice panel. This classification, along with the $T_0 - u_z$ space in Figure 8b, can be used to determine where signatures of secondary production are likely to be found in in-situ or remote sensing data. And as more experimental studies to quantify the fragment number and temperature dependencies of these processes are done, more quantitative bounds can be established in the final adjustable parameter panel.

Code availability. No data was used in producing this manuscript. Various model version codes are available upon request.

Appendix: Notation

a_X Spheroidal axis of hydrometeor of type X

β Adjustable parameter in the sigmoidal function for the fragment number generated from shattering

c_0 Primary ice nucleation rate based upon DeMott et al. (2010)

$\mathcal{D}_v$ Diffusion coefficient of water vapor

F_{BR} Leading coefficient of the fragment number generated per collision based upon data from Takahashi et al. (1995)

F_{DS} Leading coefficient of the fragment number generated per shattering droplet as in Lawson et al. (2015)

f_{red} Factor for nucleation rate reduction

F_{RS} Leading coefficient of the fragment number per kilogram of rime as in Hallett and Mossop (1974)

γ Adjustable parameter in the sigmoidal function for the fragment number generated from shattering

ICNC In-cloud ice crystal number concentration

INP Ice-nucleating particle

K_X Gravitational collection kernel for process X

$\aleph_{BR}$ Fragment number from collisional breakup per large and small graupel number

N_d Small droplet number concentration in the parcel

$\aleph_{DS}$ Fragment number from droplet shattering per large droplet number

$\aleph_{DS}^{(coll)}$ Fragment number from collisional droplet shattering per large droplet and small ice crystal number

N_i Ice crystal number concentration in the parcel

$N_{\textbf{ice}}$ Total ice hydrometeor number within the parcel, i.e. the summation of ice crystal, small and large graupel numbers

$N_{\textbf{ice}}^{(max)}$ Maximum N_{ice} formed within the parcel during a given simulation

$N_{\textbf{INP}}^{(lim)}$ Limiting ice nucleating particle number concentration to initiate secondary production

$N_{\textbf{INP}}^{(tot)}$ Total number of ice nucleating particles within the parcel available for primary nucleation. This value is fixed by the user beforehand.

N_g Small graupel number concentration in the parcel

N_G Large graupel number concentration in the parcel

N_r Medium droplet number concentration in the parcel

N_R Large droplet number concentration in the parcel

$\aleph_{RS}$ Fragment number from rime splintering per large droplet and large or small graupel number

ρ_w Density of liquid water

$p_{fr}(t,T,r)$ Temperature-, time-, and size-dependent probability that a large droplet freezes as in Bigg (1953)

$p_{sh}(T)$ Temperature-dependent probability that a frozen large droplet shatters with $p_{sh}^{(max)}$ being the maximum of this distribution

r_X Radius of hydrometeor of type X

s_w Supersaturation with respect to liquid water in the parcel

τ_X Time delay for a hydrometeor in class X to grow by deposition, riming, or condensation to the next class

T_0 Cloud base temperature or the initial temperature of the parcel

t_{end} Time when the simulation is terminated, either because the parcel has become water subsaturated or the temperature has reached 237 K where homogeneous nucleation can occur

T_{min} Minimum temperature for collisional breakup to occur

u_z Updraft velocity of the parcel

Competing interests. The authors declare no competing interests.

Acknowledgements. S.C.S. and A.N. acknowledge funding from a NASA Earth and Space Science Fellowship (NNX13AN74H), a NASA MAP grant, and a DOE EaSM grant. C.H. acknowledges funding by the Helmholtz Association through the President's Initiative and Networking Fund (VH-NG-620) and by the Deutsche Forschungsgemeinschaft (DFG) through projects HO4612/1-1 and HO4612/1-2. No data was used in producing this manuscript. Various model version codes are available upon request.

References

Beard, K. V.: Ice initiation in warm-base convective clouds: An assessment of microphysical mechanisms, Atm. Res., 28, 125–152, doi:10.1016/0169-8095(92)90024-5, 1992.

Beheng, K. D.: Microphysical properties of glaciating cumulus clouds: Comparison of measurements with a numerical simulation, Q. J. Roy. Meteor. Soc., 113, 1377–1382, doi:10.1002/qj.49711347815, 1987.

Bigg, E. K.: The formation of atmospheric ice crystals by the freezing of droplets, Q. Jour. Roy. Meteorol. Soc., 79, 510–519, doi:10.1002/qj.49707934207, 1953.

Bogacki, P. and Shampine, L. F.: A 3(2) pair of Runge-Kutta formulas, Appl. Math. Letters, 2, 321–325, doi:10.1016/0893-9659(89)90079-7, 1989.

Borys, D. R., Lowenthal, D. H., Cohn, S. A., and Brown, W. O. J.: Mountaintop and radar measurements of anthropogenic aerosol effects on snow growth and snowfall rate, Geophys. Res. Lett., 30, doi:10.1029/2002GL016855, 2003.

Brownscombe, J. L. and Thorndike, N. S. C.: Freezing and shattering of water droplets in free fall, Nature, 220, 687–689, doi:10.1038/220687a0, 1968.

Chen, J.-P. and Lamb, D.: The theoretical basis for the parameterization of ice crystal habits: growth by vapor deposition, J. Atm. Sci., 51, 1206–1221, doi:10.1175/1520-0469, 1994.

Chubb, T. H., Jensen, J. B., Siems, S. T., and Manton, M. J.: In situ observations of supercooled liquid clouds over the Southern Ocean during the HIAPER Pole-to-Pole Observation campaigns, Geophys. Res. Lett., 40, 5280–5285, doi:10.1002/grl.50986, 2013.

Clark, P., Choularton, T. W., Brown, P. R. A., Field, P. R., Illingworth, A. J., and Hogan, R. J.: Numerical modelling of mixed-phase frontal clouds observed during the CWVC project, Q. J. R. Meteorol. Soc., 131, 1677–1693, doi:10.1256/qj.03.210, 2005.

Conen, F., Morris, C. E., Leifeld, J., Yakutin, M. V., and Alewell, C.: Biological residues define the ice nucleation properties of soil dust, Atmos. Chem. Phys., 11, 9643–9648, doi:10.5194/acp-11-9643-2011, 2011.

Connolly, P. J., Choularton, T. W., Gallagher, M. W., Bower, K. N., Flynn, M. J., and Whiteway, J. A.: Cloud-resolving simulations of intense tropical *Hector* thunderstorms: Implications for aerosol-cloud interactions, Q. J. Meteorol. Soc., 132, 3079–3106, doi:10.1256/qj.05.86, 2006a.

Connolly, P. J., Heymsfield, A. J., and Choularton, T. W.: Modelling the influence of rimer surface temperature on the glaciation of intense thunderstorms: The rime-splinter mechanism of ice multiplication, Q. J. R. Meteorol. Soc., 132, 3059–3077, doi:10.1256/qj.05.45, 2006b.

Crawford, I., Bower, K. N., Choularton, T. W., Dearden, C., Crosier, J., Westbrook, C., Capes, G., Coe, H., Connolly, P. J., Dorsey, J. R., Gallagher, M. W., Williams, P., Trembath, J., Cui, Z., and Blyth, A.: Ice formation and development in aged, wintertime cumulus over the UK: observations and modelling, Atmos. Chem. Phys., 12, 4963–4985, doi:10.5194/acp-12-4963-2012, 2012.

DeMott, P. J., Prenni, A. J., Liu, X., Kreidenweis, S. M., Petters, M. D., Twomy, C. H., Richardson, M. S., Eidhammer, T., and Rogers, D. C.: Predicting global atmospheric ice nuclei distributions and their impacts on climate, Proc. Nat. Acad. Sci., 107, 11 217–11 222, doi:10.1073/pnas.0910818107, 2010.

DeMott, P. J., Hill, T. C. J., McCluskey, C. S., Prather, K. A., Collins, D. B., Sullivan, R. C., Ruppel, M. J., Mason, R. H., Irish, V. E., Lee, T., Hwang, C. Y., Rhee, T. S., Snider, J. R., McMeeking, G. R., Dhaniyala, S., Lewis, E. R., Wentzell, J. J. B., Abbatt, J., Lee, C., Sultana, C. M., Ault, A. P., Axson, J. L., Martinez, M. D., Venero, I., Santo-Figueroa, G., Stokes, M. D., Deane, G. B., Mayol-Bracero, O. L., Grassian, V. H., Bertram, T. H., Bertram, A. K., Moffett, B. F., and Franc, G. D.: Sea spray aerosol as a unique source of ice nucleating particles, Proc. Nat. Acad. Sci., 113, 5797–5803, doi:10.1073/pnas.1514034112, 2015.

Fan, J., Leung, L. R., Rosenfeld, D., Chen, Q., Li, Z., Zhang, J., and Yan, H.: Microphysical effects determine macrophysical response for aerosol impacts on deep convective clouds, Proc. Nat. Acad. Sci., 110, E4581–4590, doi:10.1073/pnas.1316830110, 2013.

Field, P., Lawson, P., Brown, G., Lloyd, C., Westbrook, D., Moisseev, A., Miltenberger, A., Nenes, A., Blyth, A., Choularton, T., Connolly, P., Bühl, J., Crosier, J., Cui, Z., Dearden, C., DeMott, P., Flossmann, A., Heymsfield, A., Huang, Y., Kalesse, H., Kanji, Z., Korolev, A., Kirchgaessner, A., Lasher-Trapp, S., Leisner, T., McFarquhar, G., Phillips, V., Stith, J., and Sullivan, S.: Chapter 7: Secondary ice production - current state of the science and recommendations for the future, Meteor. Monogr., doi:10.1175/AMSMONOGRAPHS-D-16-0014.1, 2017.

Field, P. R., Wood, R., Brown, P. R. A., Kaye, P. H., Hirst, E., Greenaway, R., and Smith, J. A.: Ice particle interarrival times measured with a fast FSSP, J. Atm. Ocean. Tech., 20, 249–261, doi:10.1175/1520-0426(2003)020, 2003.

Fridlind, A. M., Ackerman, A. S., McFarquhar, G., Zhang, G., Poellot, M. R., DeMott, P. J., Prenni, A. J., and Heymsfield, A. J.: Ice properties of single-layer stratocumulus during the Mixed-Phase Arctic Cloud Experiment: 2. Model results., J. Geophys. Res., 112, doi:10.1029/2007/JD008646, 2007.

Fröhlich-Nowoisky, J., Kampf, C. J., Weber, B., Huffman, J. A., Pöhlker, C., Andreae, M. O., Lang-Yona, N., Burrows, S. M., Gunthe, S. S., Elbert, W., Su, H., Hoor, P., Thines, E., Hoffmann, T., Despés, V., and Pöschl, U.: Bioaerosols in the Earth system: Climate, health, and ecosystem interactions, Atm. Res., 182, 346–376, doi:10.1016/j.atmosres.2016.07.018, 2016.

Hallett, J. and Mossop, S. C.: Production of secondary ice particles during the riming process, Nature, 249, 26–28, doi:10.1038/249026a0, 1974.

Heymsfield, A. and Willis, P.: Cloud conditions favoring secondary ice particle production in tropical maritime convection, J. Atmos. Sci., 71, 4500–4526, doi:10.1175/JAS-D-14-0093.1, 2014.

Heymsfield, A. J.: On measurements of small ice particles in clouds, Geophys. Res. Lett., 34, doi:10.1029/2007GL030951, 2007.

Heymsfield, A. J. and Mossop, S. C.: Temperature dependence of secondary ice crystal production during soft hail growth by riming, Quart. J. R. Met. Soc., 110, 765–770, doi:10.1002/qj.49711046512, 1984.

Hobbs, P. V. and Rangno, A. L.: Ice particle concentrations in clouds, J. Atmos. Sci., 42, 2523–2549, 1985.

Hobbs, P. V. and Rangno, A. L.: Rapid development of high ice particle concentrations in small polar maritime cumuliform clouds, J. Atmos. Sci., 47, 2710–2722, doi:10.1175/1520-0469, 1990.

Hoose, C. and Möhler, O.: Heterogeneous ice nucleation on atmospheric aerosols: a review of results from laboratory experiments, Atmos. Chem. Phys., 12, 12 531–12 621, doi:10.5194/acpd-12-12531-2012, 2012.

Huang, Y., Blyth, A. M., Brown, P. R. A., Choularton, T. W., and Cui, Z.: Factors controlling secondary ice production in cumulus clouds, Q. J. Roy. Met. Soc., doi:10.1002/qj.2987, 2017.

Huffman, J. A., Prenni, A. J., DeMott, P. J., Pöhlker, C., Mason, R. H., Fröhlich-Nowoisky, J., Tobo, Y., Despr'es, V. R., Garcia, E., Gochis, D. J., Harris, E., Mü-Germann, I., Ruzene, C., Schmer, B., Sinha, B., Day, D. A., Andreae, M. O., Jimenez, J. L., Gallagher, M., Kreidenweis, S. M., Bertram, A. K., and Pöschl, U.: High concentrations of biological aerosol particles and ice nuclei during and after rain, Atmos. Chem. Phys., 13, 6151–6164, doi:10.5194/acp-13-6151-2013, 2013.

Johnson, D. A. and Hallett, J.: Freezing and shattering of supercooled water drops, Q. J. Roy. Met. Soc., 209, 468–482, doi:10.1002/qj.49709440204, 1968.

Klett, J. D. and Davis, M. H.: Theoretical collision efficiencies of cloud droplets at small Reynolds numbers, J. Atm. Sci., pp. 107–117, doi:10.1175/1520-0469% 281973% 29030<0107% 3ATCEOCD>2.0.CO% 3B2, 1973.

Koenig, L. R.: The glaciating behavior of small cumulonimbus clouds, J. Atm. Sci., 20, 29–47, doi:10.1175/1520-0469(1963)020<0029:TGBOSC>2.0.CO;2, 1963.

Koenig, L. R.: Drop freezing through drop breakup, J. Atm. Sci., 22, 448–451, doi:10.1175/1520-0469(1965)022<0448:DFTDB>2.0.CO;2, 1965.

Koren, I., Kaufman, Y. J., Rosenfeld, D., Remer, L. A., and Rudich, Y.: Aerosol invigoration and restructuring of Atlantic convective clouds, Geo. Res. Lett., 32, doi:10.1029/2005GL023187, 2005.

Korolev, A. V. and Field, P. R.: Assessment of the performance of the inter-arrival time algorithm to identiy ice shattering artifacts in cloud particle probe measurements, Atm. Meas. Tech., 8, 761–777, 2015.

Korolev, A. V., Bailey, M. P., Hallett, J., and Isaac, G. A.: Laboratory and in-situ observation of deposition growth of frozen drops, J. App. Meteor., 43, 612–622, doi:10.1175/1520-0450(2004)043<0612:LAISOO>2.0.CO;2, 2004.

Korolev, A. V., Emery, E. F., Strapp, J. W., Cober, S. G., and Isaac, G. A.: Quantification of the effects of shattering on airborne ice particle measurements, J. Atm. Ocean. Tech., 30, 2527–2553, doi:10.1175/JTECH-D-13-00115.1, 2013.

Ladino, L. A., Korolev, A., Heckman, I., Wolde, M., Fridlind, A. M., and Ackerman, A. S.: On the role of ice-nucleating aerosol in the formation of ice particles in tropical mesoscale convective systems, Geophys. Res. Lett., 44, 1574–1582, doi:10.1002/2016GL072455, 2017.

Lance, S., Shupe, M. D., Feingold, G., Brock, C. A., Cozic, J., Holloway, J. S., Moore, R. H., Nenes, A., Schwarz, J. P., Spackman, J. R., Froyd, K. D., Murphy, D. M., Brioude, J., Cooper, O. R., Stohl, A., and Burkhart, J. F.: Cloud condensation nuclei as a modulator of ice processes in Arctic mixed-phase clouds, Atmos. Chem. Phys., 11, 8003–8015, doi:10.5194/acp-11-8003-2011, 2011.

Lasher-Trapp, S., Leon, D. C., DeMott, P. J., Villanueva-Birriel, C. M., Johnson, A. V., Moser, D. H., Tully, C. S., and Wu, W.: A multisensor investigation of rime splintering in tropical maritime cumuli, J. Atm. Sci., 73, 2547–2564, doi:10.1175/JAS-D-15-0285.1, 2016.

Lawson, R. P., Woods, S., and Morrison, H.: The microphysics of ice and precipitation development in tropical cumulus clouds, J. Atm. Sci., 72, 2429–2445, doi:10.1175/JAS-D-14-0274.1, 2015.

Leisner, T., Pander, T., Handmann, P., and Kiselev, A.: Secondary ice processes upon heterogeneous freezing of cloud droplets, 14th Conf. on Cloud Physics and Atmospheric Radiation, Amer. Meteor. Soc, Boston, MA, 2014.

Lohmann, U.: Anthropogenic aerosol influences on mixed-phase clouds, Curr. Clim. Change Rep., doi:10.1007/s40641-017-0059-9, 2017.

Mason, B. J.: The rapid glaciation of slightly supercooled cumulus clouds, Q. J. R. Meteorol. Soc., 122, 357–365, doi:10.1002/qj.49712253003, 1996.

Mason, B. J. and Maybank, J.: The fragmentation and electrification of freezing water drops, Q. J. Roy. Met. Soc., 86, 176–185, doi:10.1002/qj.49708636806, 1960.

McFarquhar, G. M., Um, J., Freer, M., Baumgardner, D., Kok, G. L., and Mace, G.: Importance of small ice crystals to cirrus properties: Observations from Tropical Warm Pool International Cloud Experiment (TWP-ICE), Geophys. Res. Lett., 34, doi:10.1029/2007GL029865, 2007.

Mizuno, H. and Matsuo, T.: Collision between graupel particles: A field observation and theory, J. Meteorol. Soc. Jap, 70, 1037–1043, doi:10.2151/jmsj1965.70.6_1037, 1992.

Möhler, O., Georgakopoulos, D. G., Morris, C. E., Benz, S., Ebert, V., Hunsmann, S., Saathoff, H., Schnaiter, M., and Wagner, R.: Heterogeneous ice nucleation activity of bacteria: new laboratory experiments at simulated cloud conditions, Biogeosciences, 5, 1425–1435, doi:10.5194/bg-5-1425-2008, 2008.

Morris, C. E., Conen, F., Huffman, J. A., Phillips, V., Pöschl, U., and Sands, D. C.: Bioprecipitation: a feedback cycle linking Earth history, ecosystem dynamics and land use through biological ice nucleators in the atmosphere, Global Change Bio., 20, 341–351, doi:10.1111/gcb.12447, 2014.

Mossop, S. C.: The influence of drop size distribution on the production of secondary ice particles during graupel growth, Q. J. R. Met. Soc., 104, 323–330, doi:10.1002/qj.49710444007, 1978.

Mossop, S. C.: Secondary ice particle production during rime growth: The effect of drop size distribution and rimer velocity, Q. J. R. Meteorol. Soc., 111, 1113–1124, doi:10.1002/qj.49711147012, 1985.

O'Sullivan, D., Murray, B. J., Ross, J. F., Whale, T. F., Price, H. C., Atkinson, J. D., Umo, N. S., and Webb, M. E.: The relevance of nanoscale biological fragments for ice nucleation in clouds, Sci. Rep., 5, doi:10.1038/srep08082, 2015.

Paukert, M., Hoose, C., and Simmel, M.: Redistribution of ice nuclei between cloud and rain droplets: Parameterization and application to deep convective clouds, J. Adv. Mod. Earth Sys., 9, 514–535, doi:10.1002/2016MS000841, 2017.

Phillips, V. T. J., Blyth, A. M., Brown, P. R. A., Choularton, T. W., and Latham, J.: The glaciation of a cumulus cloud over New Mexico, Q. J. R. Meteor. Soc., 127, 1513–1534, doi:10.1002/qj.49712757503, 2001.

Rangno, A. L. and Hobbs, P. V.: Ice particle concentrations and precipitation development in small polar maritime cumuliform clouds, Q. J. R. Meteorol. Soc., 117, 207–241, doi:10.1002/qj.49711749710, 1991.

Rangno, A. L. and Hobbs, P. V.: Ice particle concentrations and precipitation development in small continental cumuliform clouds, Q. J. R. Meteorol. Soc., 120, 573–601, doi:10.1002/qj.49712051705, 1994.

Rangno, A. L. and Hobbs, P. V.: Ice particles in stratiform clouds in the Arctic and possible mechanisms for the production of high ice concentrations, J. Geophys. Res., 106, 15 065–15 075, doi:10.1029/2000JD900286, 2001.

Rogers, D. C., DeMott, P. J., Kreidenweis, S. M., and Chen, Y.: Measurements of ice nucleating aerosols during SUCCESS, Geophys. Res. Lett., 25, 1383–1386, doi:doi/10.1029/97GL03478, 1998.

Rosenbrock, H. H.: Some general impliciat processes for the numerical solution of differential equations, The Comp. Jour., 5, 329–330, doi:10.1093/comjnl/5.4.329, 1963.

Scott, B. C. and Hobbs, P. V.: A theoretical study of the evolution of mixed-phase cumulus clouds, J. Atmos. Sci., 34, 812–826, doi:10.1175/1520-0469(1977)034<0812:ATSOTE >2.0.CO;2, 1977.

Steinke, I., Funk, R., Busse, J., Iturri, A., Kirchen, S., Leue, M., Möhler, O., Schwartz, T., Schnaiter, M., Sierau, B., Toprak, E., Ullrich, R., Ulrich, A., Hoose, C., and Leisner, T.: Ice nucleation activity of agricultural soil dust aerosols from Mongolia, Argentina, and Germany, Jour. Geophys. Res., 121, 13 559–13 576, doi:10.1002/2016JD025160, 2016.

Sullivan, S., Hoose, C., and Nenes, A.: Investigating the contribution of secondary production to ice crystal number concentrations, J. Geophys. Res., doi:10.1002/2017JD026546, 2017.

Takahashi, C.: Relation between the deformation and the crystalline nature of frozen water drops, J. Meteorol. Soc. Jap., 54, 448–453, 1976.

Takahashi, T., Nagao, Y., and Kushiyama, Y.: Possible high ice particle production during graupel-graupel collisions, J. Atmos. Sci., 52, 4523–4527, doi:10.1175/1520-0469, 1995.

Taylor, J. W., Choularton, T. W., Blyth, A. M., Liu, Z., Bower, K. N., Crosier, J., Gallagher, M. W., Williams, P. I., Dorsey, J. R., Flynn, M. J., Bennett, L. J., Huang, Y., French, J., Korolev, A., and Brown, P. R. A.: Observations of cloud microphysics and ice formation during COPE, Atmos. Chem. Phys., 16, doi:10.5194/acp-16-799-2016, 2016.

Vardiman, L.: The generation of secondary ice particles in clouds by crystal-crystal collision, J. Atmos. Sci., 35, 2168–2180, doi:10.1175/1520-0469, 1978.

Yano, J.-I. and Phillips, V. T. J.: Ice-ice collisions: an ice multiplication process in atmospheric clouds, J. Atmos. Sci., 68, 322–333, doi:10.1175/2010JAS3607.1, 2011.

Yano, J.-I., Phillips, V. T. J., and Kanawade, V.: Explosive ice multiplication by mechanical break-up in-ice-ice collisions: a dynamical system-based study, Q. J. Roy. Met. Soc., 142, 867–879, doi:10.1002/qj.2687, 2015.